



Contents lists available at ScienceDirect

Computer Methods in Applied Mechanics and Engineering

journal homepage: www.elsevier.com/locate/cma

Packing spherical discrete elements for large scale simulations

Jean-François Jerier^a, Vincent Richefeu^a, Didier Imbault^a, Frédéric-Victor Donzé^{a,b,*}^a Laboratoire Sols, Solides, Structures et Risques, UMR5521, Université Joseph Fourier, INP, Grenoble Université, Domaine Universitaire, BP 53, 38041 Grenoble Cedex 9, France^b CSIRO Earth Science and Resource Engineering, Queensland Centre for Advanced Technologies, 1 Technology Court, Pullenvale, 4069, Australia

ARTICLE INFO

Article history:

Received 8 July 2009

Received in revised form 18 January 2010

Accepted 25 January 2010

Available online 1 March 2010

Keywords:

Discrete element method

Sphere packing

Tetrahedral mesh

ABSTRACT

We introduce a new geometric method to generate sphere packings with restricted overlap values. Sample generation is an important, but time-consuming, step that precedes a calculation performed with the discrete element method (DEM). At present, there does not exist any software dedicated to DEM which would be similar to the mesh software that exists for finite element methods (FEM). A practical objective of the method is to build very large sphere packings (several hundreds of thousands) in a few minutes instead of several days as the current dynamic methods do. The developed algorithm uses a new geometric procedure to position very efficiently the polydisperse spheres in a tetrahedral mesh. The algorithm, implemented into YADE-OPEN DEM (open-source software), consists in filling tetrahedral meshes with spheres. In addition to the features of the tetrahedral mesh, the input parameters are the minimum and maximum radii (or their size ratio), and the magnitude of authorized overlaps. The filling procedure is stopped when a target solid fraction or number of spheres is reached. Based on this method, an efficient tool can be designed for DEMs used by researchers and engineers. The generated packings can be isotropic and the number of contacts per sphere is very high due to its geometric procedure. In this paper, different properties of the generated packings are characterized and examples from real industrial problems are presented to show how this method can be used. The current C++ version of this packing algorithm is part of YADE-OPEN DEM [20] available on the web (<https://yade-dem.org>).

© 2010 Elsevier B.V. All rights reserved.

1. Introduction

The discrete element method (DEM) [7] is a powerful tool to simulate granular media. These media (concretes, [5,23,28], ceramics [40], powders [24], soils [9,31]) are often represented by random packing of spheres which exhibit specific properties such as solid fraction, particle connectivity, particle size distribution and fabric. The discrete element simulations need sphere packings generated with chosen geometric properties (that can be similar or not to the real granular media). In a broad sense, two types of packing constructions exist: the dynamic approach and the geometric approach.

The first approach is based on dynamic simulations. It is commonly used for example to prepare numerical samples for the study of soil [3,30,38], concrete [39], powders [10], Van Der Waals forces [45], or cohesion [32,33,36]. The main dynamic methods described in the literature are the iterative growth algorithm [22,41] and the isotropic compression [2,25]. These dynamic methods can satisfactorily reproduce the real packing properties [21,44], but require high time-consuming computation.

Unlike dynamic approaches, geometric methods can be used to quickly build large samples. In fact, assembling a packing of 10,000 spheres may take several days with dynamics methods, while the same project can be made 'geometrically' in a few minutes. In return, the sample is not stable from a mechanical point of view and it contains no information on the contact forces between the particles. However, even if the resulting configurations are not stable, they are close enough to a mechanically acceptable state. Different geometric algorithms were developed to generate sphere assemblies for example in cylindrical [29], cubical [16] or conical [18] containers. The well-known ballistic deposition algorithm [1,17,18] consists in adding spheres one by one in a geometrically stable position at the surface of an evenly packed set of spheres. The texture of the packing can be controlled when using this very efficient method [42], but dynamic algorithms show some limitations when producing complex shapes.

In this paper, a dense and polydisperse sphere packing algorithm is presented. This new algorithm is of great interest for engineering problems since very large packings can be built in a few minutes starting from a tetrahedral mesh. This tool is an extension of a recently developed geometric algorithm [15]. Since the advent of intensive computation, the DEM became an interesting alternative tool to study large deformation processes in materials. In this DEM-based method [7,9], it is assumed that materials can be approximated as assemblies of discrete elements bonded together by different models of cohesive forces; the overall mechanical behavior can be evaluated through the

* Corresponding author. Laboratoire Sols, Solides, Structures et Risques, UMR5521, Université Joseph Fourier, INP, Grenoble Université, Domaine Universitaire, BP 53, 38041 Grenoble Cedex 9, France.

E-mail address: Frederic.Donze@hmg.inpg.fr (F.-V. Donzé).

collective contributions of these discrete elements under loading or unloading processes exhibiting motion, displacement, sliding, inter-element rotation and where de-bonding mimics the nucleation of cracks [14]. Most of the DEMs use spherical elements because only a single value, the radius, is required to define the geometry of the elements and there is only one possible type of contact among elements, which can be detected easily. As a result, computer memory requirements and computer processing time are minimized with these particle shapes and in addition a large number of particles can be analyzed.

In the Section 2, we present a step by step algorithm to generate isotropic samples of polydisperse spheres starting from tetrahedral meshes. Different packing properties will then be characterized in Section 3. These properties include the solid fraction, the connectivity, the fabric and order of the packing. The computing time is also characterized for the C++ version of the code. In the last part, the developed algorithm will be applied to different engineering cases to illustrate the abilities of this tool. We emphasize that this method should not be appropriated for granular materials modeled at the real particle scale, since crucial characteristics such as the texture or the size distribution cannot be directly monitored. Hence, the sphere packing generated by the geometric algorithm presented in this paper should only be dedicated to reproduce the simulated material at the macroscopic scale.

2. Algorithm description

The developed geometric algorithm is based on tetrahedral meshes generated by meshing softwares such as Ghs3D [12], Gmsh [13] or Netgen [35]. Each tetrahedron is progressively filled with the following constraints: (i) the sphere radii range from r_{\min} to r_{\max} , (ii) the sphere overlaps are limited to a given value $\delta_n^{\max} = -\varepsilon r_{\min}$, where ε is the maximum overlap rate. The tetrahedral mesh and these constraint parameters both correspond to the input data that must be supplied by the user. The key *geometric procedure* consists in placing one sphere in contact with four non-coplanar spheres. The first version of this geometric procedure was based on the inversion function [4]. In the current version, an equation system for a sphere intersection with four spheres (see Eqs. (1)–(4) below) is solved.

2.1. Geometric procedure

In order to place a sphere in contact with four other spheres, two different geometric procedures are implemented in the code. The first procedure, described in detail in [15], is based on *geometric inversion*. The new geometric procedure has proven to be faster. It is based on solving a system of equations that translates the intersection of a fifth sphere with four existing spheres:

$$(x-x_1)^2 + (y-y_1)^2 + (z-z_1)^2 = (r+r_1)^2, \quad (1)$$

$$(x-x_2)^2 + (y-y_2)^2 + (z-z_2)^2 = (r+r_2)^2, \quad (2)$$

$$(x-x_3)^2 + (y-y_3)^2 + (z-z_3)^2 = (r+r_3)^2, \quad (3)$$

$$(x-x_4)^2 + (y-y_4)^2 + (z-z_4)^2 = (r+r_4)^2, \quad (4)$$

where x, y and z are the coordinates of the added sphere, r is its radius, subscript 1, 2, 3 and 4 denote for the four spheres ever placed. A relation can easily be written by subtracting Eqs. (1)–(4) from one another:

$$\mathbb{A}\mathbf{x} = \mathbf{b}(r), \quad (5)$$

where:

$$\mathbb{A} = 2 \begin{bmatrix} (x_1-x_2) & (y_1-y_2) & (z_1-z_2) \\ (x_1-x_3) & (y_1-y_3) & (z_1-z_3) \\ (x_1-x_4) & (y_1-y_4) & (z_1-z_4) \end{bmatrix}, \quad (6)$$

$$\mathbf{x} = \begin{bmatrix} x \\ y \\ z \end{bmatrix}, \quad (7)$$

$$\mathbf{b}(r) = \begin{bmatrix} (x_1^2 + y_1^2 + z_1^2 - r_1^2) - (x_2^2 + y_2^2 + z_2^2 - r_2^2) - 2r(r_1 - r_2) \\ (x_1^2 + y_1^2 + z_1^2 - r_1^2) - (x_3^2 + y_3^2 + z_3^2 - r_3^2) - 2r(r_1 - r_3) \\ (x_1^2 + y_1^2 + z_1^2 - r_1^2) - (x_4^2 + y_4^2 + z_4^2 - r_4^2) - 2r(r_1 - r_4) \end{bmatrix}. \quad (8)$$

In Eq. (5) the vector \mathbf{x} corresponds to the coordinates of the fifth sphere, and the right-hand member vector \mathbf{b} depends on r . When a solution exists (i.e. $\det(\mathbb{A}) \neq 0$, which is not true when the four spheres are coplanar for example), it is expressed as a function of r so that

$$\mathbf{x} = \mathbb{A}^{-1}\mathbf{b}(r) = r\mathbf{x}_a + \mathbf{x}_b. \quad (9)$$

where \mathbf{x}_a and \mathbf{x}_b are known vectors. Otherwise, the procedure is stopped. In addition to being faster, this procedure is also able to detect very quickly a failing sphere insertion. By including Eq. (9) in Eq. (1), we obtain a second order equation that allows us to evaluate one or two candidate value(s) of radius r . If r does not satisfy the predefined radius range or if at least one overlap with any sphere of the packing exceeds the value prescribed by the user, the position and radius of the fifth sphere are rejected. Although one unique solution exists and therefore the involved spheres in Eq. (9) do not overlap, the fifth sphere can interpenetrate another sphere of the packing. In last resort, the radius of placed sphere can be decreased to cancel any overlap. To avoid a too weak connectivity due to the radius reduction, the fifth sphere is also rejected when it is not in contact with at least z_{\min} other spheres (with $z_{\min} = 2, 3$ or 4).

As we shall see in the next section, most of the added spheres are inserted via the geometric procedure during the padding. In short, the method consists in estimating roughly a loci $p(x_p, y_p, z_p)$ where a sphere could be added, and using the geometric procedure to put it in contact with the four nearest packed spheres. Nevertheless, the estimated loci are sometimes so coarse that the procedure fails. To increase the chances of placing a sphere close to p , a list of spheres sorted from nearest to farthest [11] is used to build several four-spheres sets. The geometric procedure is then applied with these sets until it can be placed in agreement with the user constraints.

2.2. Sphere packing method

As stated before, the packing method uses a tetrahedral mesh to generate an assembly of spheres. In this mesh, the mean length of edges approximately corresponds to 8 times the mean radius of the spheres. In this section, we detail the packing generation process step by step from a simple example based on the filling of a cubic tetrahedral mesh (step 1 in Fig. 1)

In the next two steps, spheres are directly added at the middle edges and at the nodes (respectively, step 2 and step 3 in Fig. 1). The radius of all middle-edge spheres is set as a function of the length ℓ of the corresponding edge ($r = \ell/8$), and the radius of all node spheres is set to the length ℓ_s of the smallest adjacent edge ($r = \ell_s$). If the radius is over r_{\max} , a value is randomly chosen in the predefined range. If the radius is below r_{\min} , its value is set to r_{\min} . After the third step, spheres can overlap. A routine is then used to reduce iteratively the radii of overlapping spheres so that the overlap satisfies the

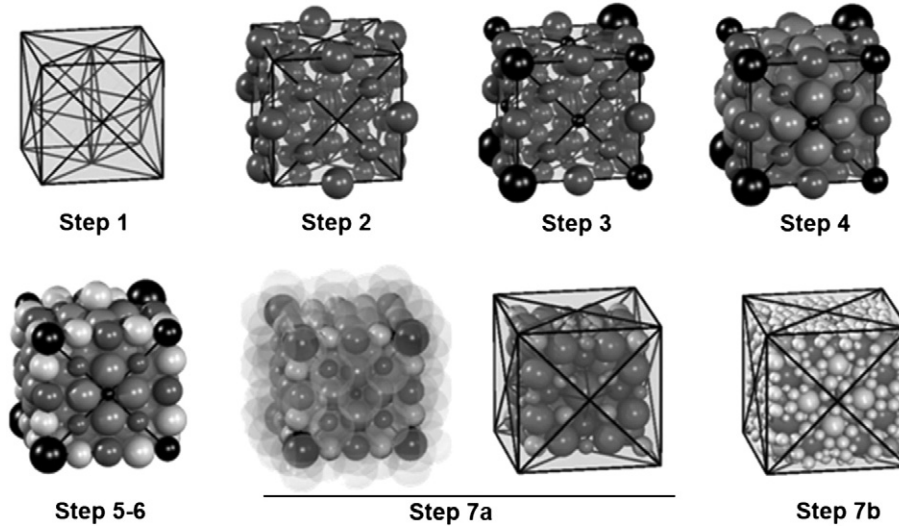


Fig. 1. The different steps of the packing method.

maximum accepted value. The spheres with a radius smaller than r_{\min} are removed.

In all the next steps, the spheres are added via the geometric procedure by giving a rough estimate of their locus (see Section 2.1). We first target the barycenter of each triangular face and tetrahedron of the mesh (step 4 and step 5 in Fig. 1). We then target the loci midway between the barycenter and the four nodes of each tetrahedron (step 6 in Fig. 1). At the end of these steps, the solid fraction of the packing is generally lower than 0.55 and the mean number of contact per sphere (coordination number) is about 5. The total number of spheres N is about $10 \times$ the number of tetrahedra N_t in the mesh. A looser packing can be obtained if steps 5 and 6 are not performed. In this case the solid fraction is about 0.45 with a coordination number larger than z_{\min} used in the geometric procedure.

At this point, the packing does not respect the mesh boundaries as we can see in Fig. 1 (steps 5 and 6). To model the convex boundaries of the packing, virtual spheres (i.e. spheres not included in the final packing) are placed tangent to the external side of the triangular boundary faces of the mesh (Fig. 2). Their radii are set large enough to approach at best a plane. Packed spheres that overlap the virtual spheres (within the given error) are then suppressed as shown in Fig. 1 (step 7a).

In order to increase the density of the whole packing and to fill spheres in the gaps close to the mesh boundaries (created by removing boundary spheres), we detect ‘void spaces’ where new spheres could be added by applying the geometric procedure. Practically, void spaces are tetrahedra resulting from a tridimensional Delaunay triangulation built with the sphere centers. Note that each tetrahedron element in the triangulation is determined by four

mutually nearest spheres centered at the vertices. We use the CGAL library [6] that provides very efficient template functions to build a Delaunay triangulation. From this point on, the tetrahedra of the mesh are no longer needed, and the tetrahedra in question are those from the triangulation. A homogeneous density of the packing can be obtained by filling first the largest void spaces. For this reason and also to optimize the filling step (step 7b), void spaces V_v^t associated with each tetrahedron t must be determined and then sorted from largest to smallest. These volumes are given by:

$$V_v^t = V_t - \sum_{i=1}^4 \left(\frac{S_i^t}{S_i} V_i \right), \quad (10)$$

where V_t is the volume of the tetrahedron, V_i and S_i are respectively the volume and the surface of the spheres at the vertices of the tetrahedron, and S_i^t are the surfaces of the spherical triangle for spheres i equal to

$$S_i^t = (\alpha + \beta + \gamma - \pi) r_i^2, \quad (11)$$

with

$$\alpha = \arccos \left(\frac{\cos a - \cos b \cos c}{\sin b \sin c} \right), \quad (12)$$

$$\beta = \arccos \left(\frac{\cos b - \cos c \cos a}{\sin c \sin a} \right), \quad (13)$$

$$\gamma = \arccos \left(\frac{\cos c - \cos a \cos b}{\sin a \sin b} \right). \quad (14)$$

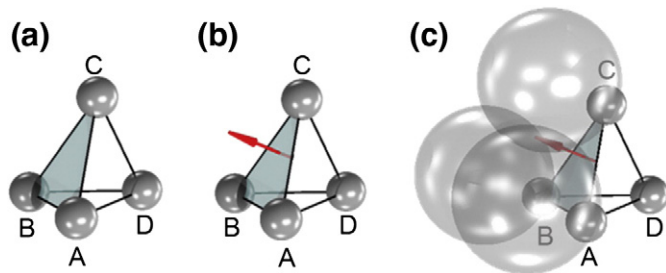


Fig. 2. Placement of the virtual spheres. (a) The triangular faces that belong to only one tetrahedron are marked as boundary faces. (b) Outgoing normal is computed for each boundary face by using the position of the fourth sphere. (c) The virtual spheres are added outside the borders, at the nodes and the center of the face (not shown for sake of readability), taking care that they are not duplicated.

In Eqs. (12)–(14), a, b, c are the three circular arc lengths that result from the intersection of a tetrahedron with a sphere placed at a vertex (spherical triangle, see Fig. 3(b)).

In the last step (step 7b), referred to *in search of void spaces*, the Delaunay triangulation and the void filling (see Fig. 3) are iteratively applied to make the packing denser. If these iterations are repeated until no more sphere can be added, the maximum solid fraction, according to the chosen radius range, will be reached. However, the user can define a stop criterion based on a target solid fraction ϕ_0 or a total number of spheres N_0 in the packing. These criteria must be checked *during* the iterative filling procedure because the parameters ϕ and N evolve very quickly. The search for void spaces is usually applied to the whole packing but it can also be applied only to a given

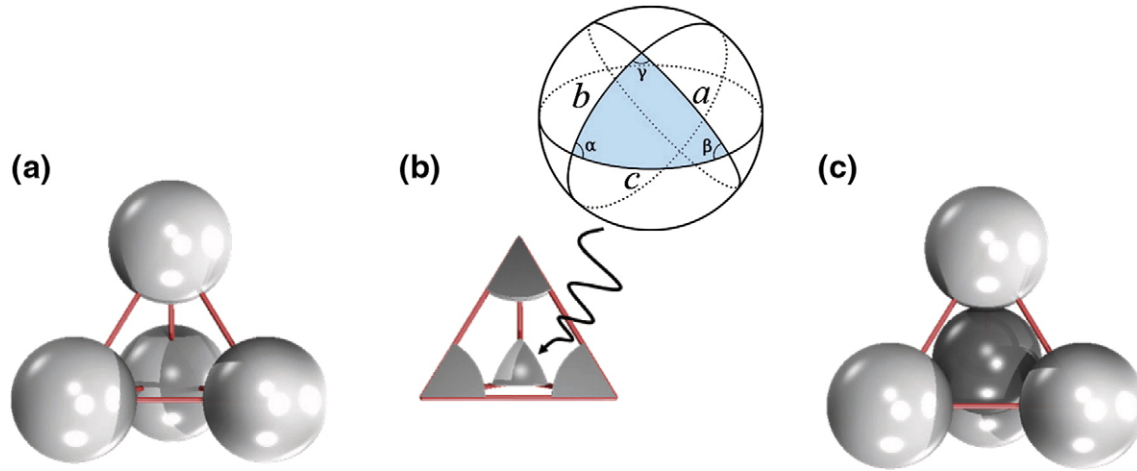


Fig. 3. Detection and reduction of void space in a tetrahedron formed by four spheres. (a) Tetrahedral mesh created by the Delaunay algorithm on the four spheres in the stack. (b) Representation of a spherical triangle on a sphere placed at the tetrahedron vertex. (c) Positioning of a sphere in contact (with at least z_{min} contacts) with four neighboring spheres to fill the empty space.

region. By defining different regions with different solid fractions it is thus possible to obtain a gradient of density (solid fraction).

3. Characterization

In this section, we first characterize the structure of the generated assemblies. The method efficiency is then presented.

3.1. Packing properties

To characterize the packing, we introduce different geometric properties. The mean number of contacts per sphere, namely the coordination number z , relates to the connectivity:

$$z = \frac{1}{N} \sum_{i=1}^N z^i, \quad (15)$$

where N is the total number of spheres in the packing, and z^i is the local number of contacts for the sphere i . The filling rate is defined by the solid fraction ϕ calculated in a spherical probe:

$$\phi = \frac{1}{V_p} \sum_{i=1}^N \chi_i V_i, \quad (16)$$

where V_p is the volume of the spherical probe, and $\chi_i \in [0,1]$ is the volume fraction of the sphere i contained inside the probe. We generally observed that the coordination number z is correlated with the solid fraction ϕ in a granular packing. The generated packing must satisfy this observation. Fig. 4(a) shows the maximum solid fraction and coordination number obtained for six radius ratios $R = r_{max}/r_{min}$ (from 2 to 7) generated from the same meshed cube composed of 1112 tetrahedra. We notice that geometrically generated assemblies obey the expected correlation between ϕ and z . The high coordination number is induced by the geometric procedure which ensures that no free sphere (i.e. sphere without contact) exists. A picture of the densest packing ($R = 7$) is depicted in Fig. 5 (b).

The algorithm is also able to generate very loose packing ($\phi \approx 0.46$) with different sphere size distribution, while keeping a high enough coordination number ($z \approx 4.75$). This is shown in Fig. 4(b) where different radius ratios were used to generate sphere packings with a target solid fraction of 0.46. This value is very low and using only friction contact in a DEM simulation should not be sufficient to maintain this low density at a stabilized state. In comparison, a random loose packing gives a solid fraction $\phi \approx 0.58$. Fig. 5 (a) shows the loosest packing obtained with $R = 2$.

In polydisperse sphere packings generated by DEM computation for example, strong forces (i.e. larger than the mean force) are preferentially supported by large particles [43]. Most of the other particles transmit weak forces that hold up the strong network of forces. It is important that larger spheres are interconnected in the generated packings, because this corresponds to a state naturally reached when mechanical forces are taken into account. We checked this feature of the connectivity in the generated packing by defining a *partial coordination*

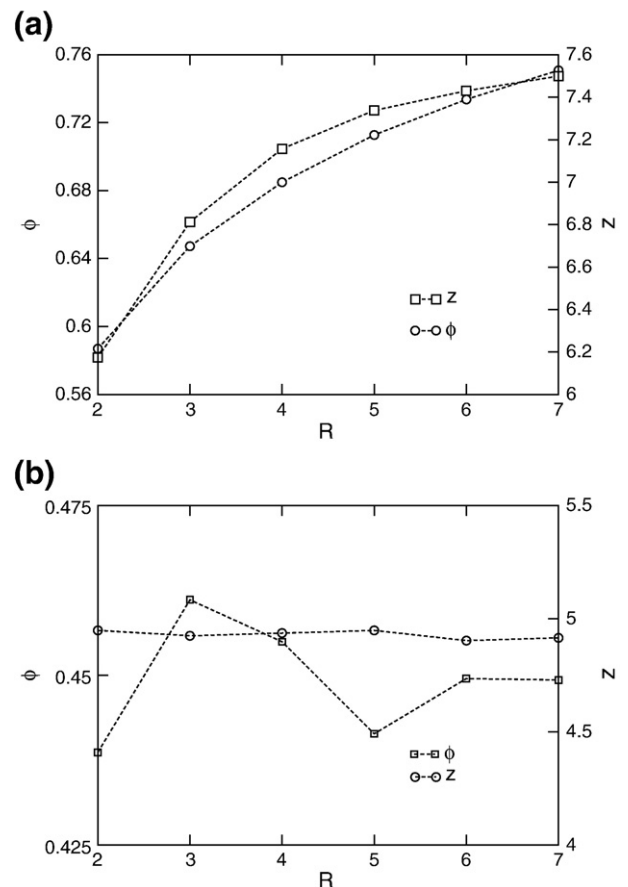


Fig. 4. A solid fraction ϕ and coordination number z as a function of the radius ratio R . The filling procedure was stopped when (a) no more sphere could be added, and (b) the targeted solid fraction ϕ_0 was reached.

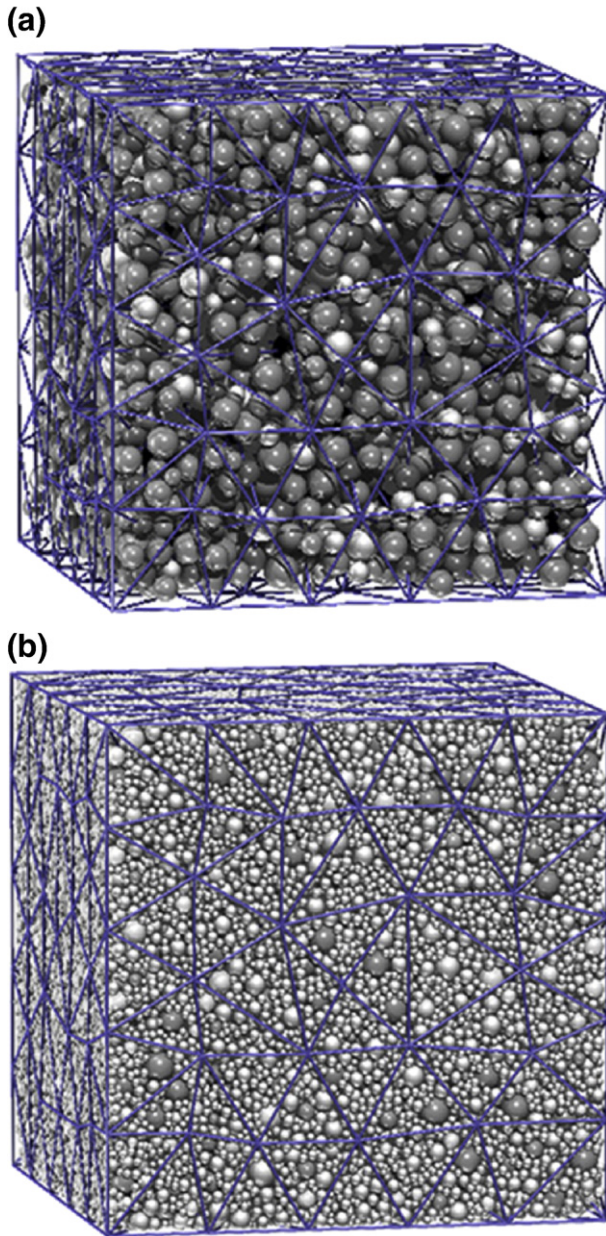


Fig. 5. Examples of generated dense packings for (a) $R=2$, and (b) $R=7$.

number $\bar{z}(\xi)$ for sphere radii greater than $r_{\min} + \xi(r_{\max} - r_{\min})$, where $\xi \in [0, 1]$. In other words, $z(\xi)$ corresponds mean number of contact per particle when the smaller spheres ($r < \xi$) are taken off. With this definition, the total coordination number of the sample is $z(\xi=0)$. Fig. 6 shows the partial coordination number together with the *probability distribution function* (pdf) of the sphere radii for a loose and a dense packing. We can see that the partial coordination number reaches a zero value only for $\xi \geq 0.9$, which corresponds in fact to a very small amount of spheres as shown by pdf. Larger spheres in significant amounts (i.e. $0.6 < \xi < 0.9$) are indeed interconnected, which shows that they are not isolated and correspond to a realistic situation.

The morphology of the contact network in an assembly can be quantified by the fabric tensor. This tensor characterizes the distribution of contact orientations. We consider here the second order fabric tensor \mathbb{F} the components of which are given by:

$$F_{\alpha\beta} = \frac{1}{N_c} \sum_{c=1}^{N_c} \mathbf{n}_\alpha^c \mathbf{n}_\beta^c, \quad (17)$$

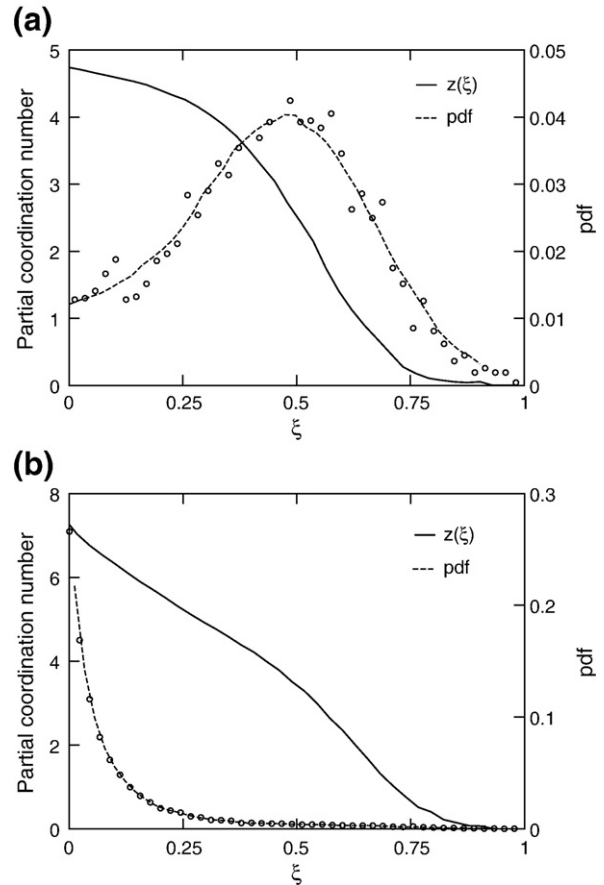


Fig. 6. Partial coordination number $z(\xi)$ and probability distribution function (pdf) of sphere radii for a loose ($\phi \approx 0.46$) (a) and a dense ($\phi \approx 0.75$) (b) packing with the radius ratio $R=7$.

where N_c is the number of contacts in the test volume V , \mathbf{n}^c is the unit vector of the contact c , and α and β are the spatial directions. The eigenvalues (F_1, F_2 and F_3) of the tensor quantify the anisotropy of the structure. A non-ordered assembly can be considered as isotropic when F_1, F_2 and F_3 are all equal to $1/3$. These eigenvalues, shown in Fig. 7(a), are almost equal with an accuracy of ± 0.02 in the worst case ($R=2$) where the possibilities of adding new spheres are limited. For the other cases ($R \geq 3$), equal values are observed with an accuracy of ± 0.01 . It will be noted in the following that a packing is not ordered for $R \geq 3$, which means that it is isotropic when $\mathbb{F} \approx (1/3)\mathbb{I}$, where \mathbb{I} is the unit tensor.

One might think intuitively that the isotropy of the packing is directly derived from the isotropy of the mesh. To test this, we stretched a mesh by multiplying the z components of the nodes by a factor 3. The resulting packing was still isotropic, which means that the mesh anisotropy does not influence the packing isotropy.

The organization of the packing can be described by means of a *radial distribution function* $g(r)$, where r is the inter-center distance. This function gives statistical information on how the spheres are radially packed around each other. More precisely, we can think of it as the average number of spheres found at a given inter-center distance in all directions. A typical shape of $g(r)$ is shown in Fig. 7(b) for quasi-monodisperse assembly ($R=1.5$). At a short distance (less than the mean diameter) the function $g(r)$ is zero because two particles cannot occupy the same space. A first peak corresponding to the spheres in contact appears at a distance r close to the mean diameter $\langle d \rangle$ of the spheres. It is followed by other peaks that become less and less marked. At long distance, $g(r)$ approaches the value 1, which indicates there is no long-range order. We observe a softening of the first peak when the ratio or the solid fraction is increased (Fig. 7(b)). Similar

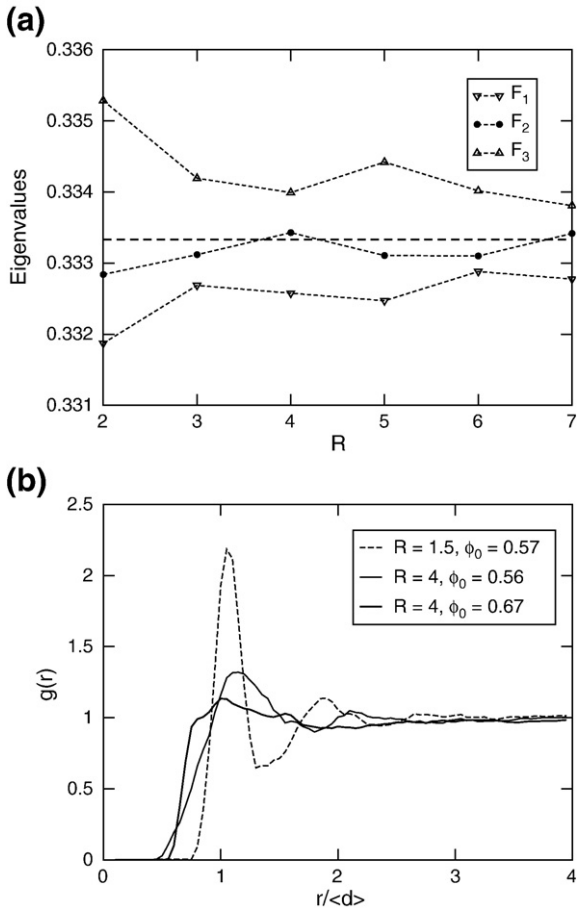


Fig. 7. (a) Eigenvalues of the fabric tensor ($F_1 < F_2 < F_3$) as a function of the radius ratio R . The dashed line corresponds to the perfectly isotropic case ($F_1 = F_2 = F_3 = 1/3$). (b) Radial distribution function $g(r)$ for different packings.

observations were made with a packing generated from stretched tetrahedra. The analysis of the radial distribution function shows that the packing generated with the method are never ordered even if the chosen size ratio is close to 1.

3.2. Efficiency of the packing generation

Until now, we have focused on the packing properties. It is also interesting to characterize the duration of the packing generation. The prototype version of the method was developed with the interpreted language MATLAB® [27]. The packings were already more efficient than those found in dynamic methods. The current C++ version is drastically faster (duration can be divided by 25 in the worst cases). The time evolves linearly with the number of tetrahedral meshes as shown in Fig. 8(a) where the target solid fraction ϕ_0 was fixed to 0.6. However, the computation time becomes exponential for high values of the solid fraction ($\phi_0 \geq 0.68$) up to a limit value depending on the radius ratio; Fig. 8(b).

Fig. 8(c) synthesizes this information with a color-map of the computation time displayed in the parameter space ($\phi - R$). The packings were done starting with a mesh of 1040 tetrahedra with almost identical sizes. We distinguish four different regions. Region 1 represents the combinations of parameters ($\phi - R$) that cannot be used. In other words, no packing can be generated with parameters picked in this region. Region 2 shows the values of ϕ and R that provide a linear computing time. In region 3, the computing time evolves exponentially as a function of ϕ . As in region 1, region 4 corresponds to packings that cannot be made directly, but the cancellation of some preliminary steps allows the algorithm to obtain these low values of ϕ . Besides, the solid fractions around 0.46 shown in Fig. 4 were obtained in this way by suppressing steps 5 and 6.

It is important to note that Fig. 8 (c) gives only an approximate definition of the four regions. Indeed, the boundaries of regions may slightly move depending on the mesh. For example, the higher solid fractions obtained from two different tetrahedral meshes are represented both on Figs. 8(c) and 4 (a), and we can observe that the values are only slightly different.

4. Examples and extensions

As stated in the introduction, the DEM can be used with appropriate force-laws to model continuous materials from a non-damaged state up to its complete failure. The discrete element approach is used with the hope of taking into account crack initiations, propagations, bifurcations and interactions. Besides formulating the correct interaction forces between elements, the first

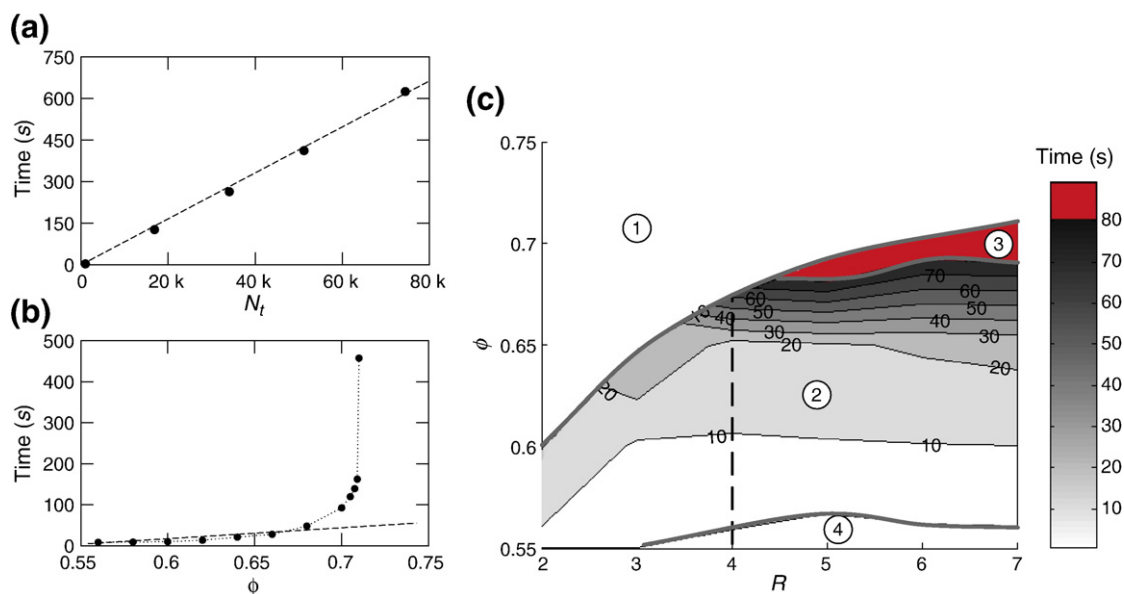


Fig. 8. Main features of the packing process duration. (a) Linear evolution of the computation time as a function of the number of tetrahedral meshes N_t . (b) First linear, then exponential, evolution of the computation time as a function of the solid fraction ϕ . (c) A map of the computing time in the parameter space ($\phi - R$).

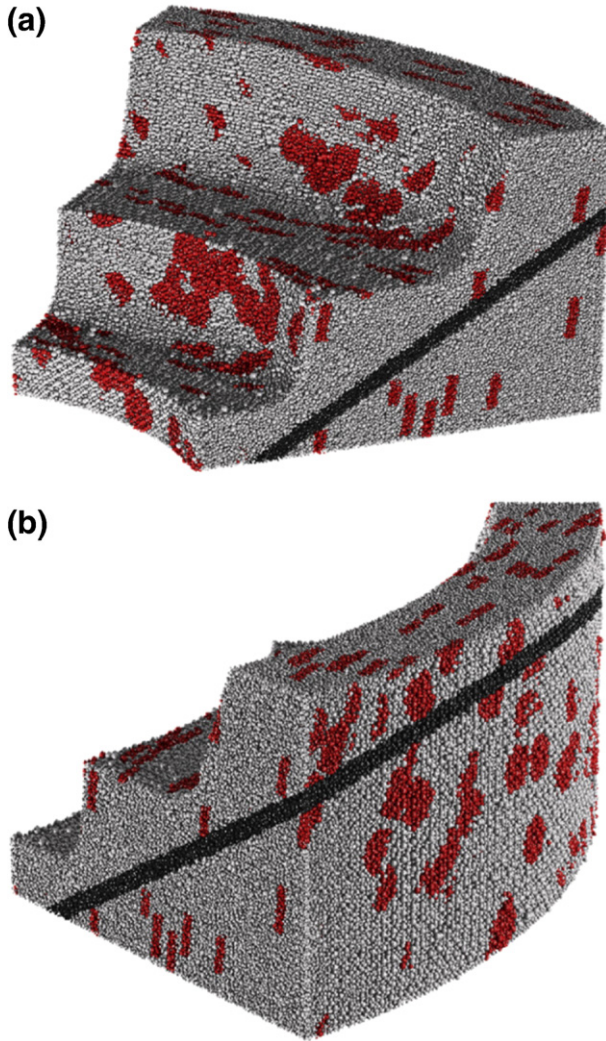


Fig. 9. A million spheres have been densely packed to represent a portion of an open pit mine, with two benches. The dark line corresponds to a fault and the colored speckles to joints.

critical point is to generate a set of discrete elements which is representative of the problem. This generally covers three things: the size of the medium, its internal organization and its boundary conditions. These criteria often involve a very time consuming initial packing generation step, and the fast generation algorithm presented here would be a useful tool for engineers and researchers. To illustrate the capabilities of this algorithm to tackle the previous points, examples are presented in the following subsections.

4.1. Large scale structures

As a first illustration of the need for a large size medium, mining excavation is an applied domain for which large scale simulation is important because it involves large discontinuous deformations of the rock mass. For example, in large open pit mines, features such as faults are relatively widely spaced and continuous along strike and dip across the entire mine site. In addition, closely spaced joints and faults that typically do not extend for more than a bench can be found. Thus, there is a need to develop 3D numerical models that can cover these different scales of discontinuities. Using the DEM, it is possible to model the strength of the intact rock and joint fabric within the rock bridges that may occur along a candidate failure surface in a closely jointed rock mass. Then, the brittle fracture that can propagate across the joint fabric within the rock bridges as the rock mass deforms, can be reproduced. However, if this mechanical description is valuable because of the local insight on instabilities that it provides, the geometrical representation of the medium is of utmost importance, since it composes the structural framework of the deformation process. The packing tool presented in this work can be used to represent the rock mass as a dense collection of discrete elements, which will be bonded together in the DEM code YADE [19]. An example of this applied 3D packing, Fig. 9 shows how a million spheres can be packed in a few minutes on a basic PC, to represent a portion of an open pit.

4.2. Composite material

One of the best known composite materials is reinforced concrete. Its behavior is greatly influenced by the coupled effect of the rebar with the surrounding concrete matrix. An advanced modeling of steel–concrete composite beams requires the explicit introduction of local interaction phenomena [8,26], since adhesion and friction between concrete and the steel surface play a major role. In DEM,

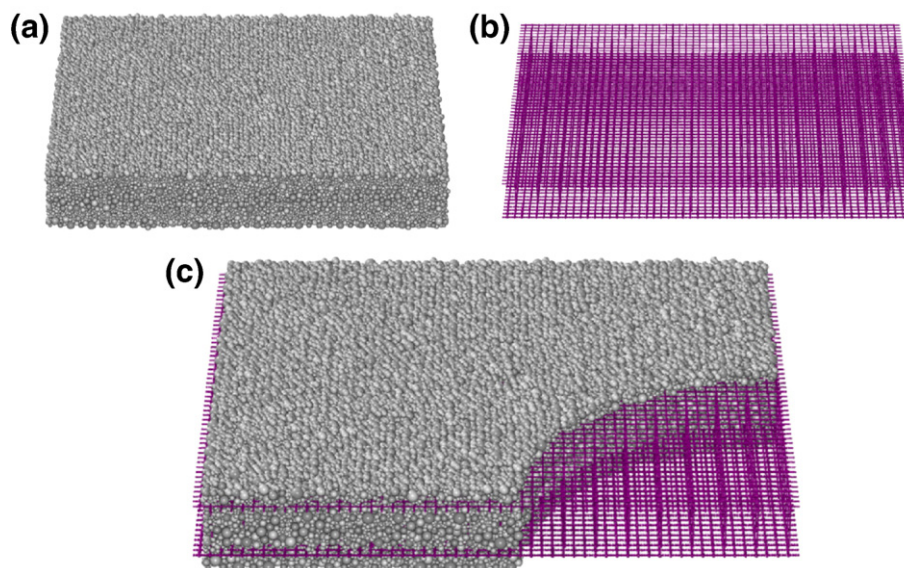


Fig. 10. A million spheres have been densely packed to represent a reinforced concrete slab. Both the concrete and the reinforcements are modeled by discrete spherical elements. Cutting was done to ease the visualization of the reinforcements.

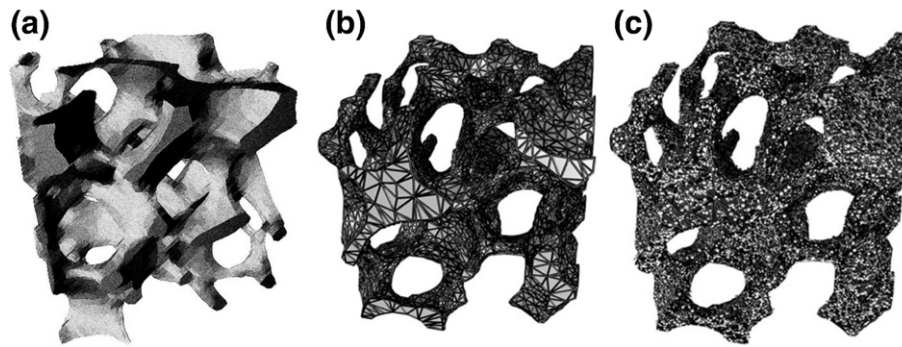


Fig. 11. Packing generation from a meshed tomography of porous ceramic. (a) Micro-structure of a porous ceramic; (b) tetrahedral mesh reconstruction; (c) packing with spheres.

the reinforcement is introduced in the model as lines of elements placed next to each other [23,37]. The diameter of the elements is that of the real reinforcement and ad hoc local behavior can be considered (generally elastic, perfectly plastic). The modeling of the steel-concrete interface by discrete elements means the definition of a particular interaction force between a steel element and a concrete element and because the reinforcement bar creates a privileged direction for rupture, the formulation of such interaction laws must be carefully chosen [34]. As an example of the geometrical set up of a reinforced concrete medium, a reinforced concrete slab obtained with the packing algorithm is presented in Fig. 10. Different basic steps are used to build such a structure. First a dense polydisperse sphere packing is obtained by using steps 1 to 5 of Section 2.2 (see Fig. 10(a)). After these spheres positioned, additional spheres that constitute the reinforcement structure are added (see Fig. 10(b)). Then, spheres that overlap the added spheres are removed just before the searching for void spaces begins. This last step ensures that the contact exists between the reinforcements and the concrete. Doing so a structure with one million spherical elements can be generated on a regular PC (see Fig. 10(c)).

4.3. Complex geometry

In the third example, we show that the method can accurately reproduce a complex geometry. We choose for this purpose, the case of a porous ceramic used for bone remodeling.

The study of ceramic behavior is a growing research field for a wide range of applications (e.g., biomaterials, powders) and recent advancements enable the production of submicrometer-grained ceramics which are free of impurities and amorphous phases at the grain boundaries. Despite these advancements, extensive use of ceramics is still limited because of their low fracture toughness. Therefore, it is essential to gain a thorough understanding of the fracture process at the microscopic level together with its relation to macroscopic behavior of the material.

A small part of this biomaterial was scanned by X-ray tomography. The resulting micro-structure is shown in Fig. 11(a). A tetrahedral mesh has been obtained by a tomographic reconstruction technique (Fig. 11(b)). Then, spheres are packed onto this mesh Fig. 11(c) and the DEM can be applied to study initiation and propagation of cracks within this biomaterial. In this case, the large assembly of spheres is obtained quickly (e.g. 1000 spheres per second with a pentium 2.33 GHz, see Fig. 8).

5. Conclusion

A new geometric packing method has been presented. It uses tetrahedral mesh to build an isotropic packing of polydisperse spheres in a short computation time. The generation procedure is very flexible in the sense that the packings can be loose or dense, with high or low connectivity according to wisely chosen parameters. The filling

procedure is mainly based on a fast geometric procedure to insert a fifth sphere into the void space between four neighboring spheres. The void spaces are first located by using the tetrahedral mesh. The packing density is then increased by filling the void spaces detected by applying a Delaunay triangulation on the sphere centers. Because the new geometric algorithm is coded in C++, it is extremely fast which is due to the use of the very efficient computational geometry algorithm library (CGAL). The method has shown its efficiency when applied to real test cases such as modeling an open-pit mine slope, a reinforced concrete slab and a porous structure scanned by X-ray tomography.

Acknowledgements

We thank J.-P. Vassal for his help with the tomographic mesh generation used in this paper. The prototype version was written with the help of S. Lignon that we would like to acknowledge too.

References

- [1] N. Aparicio, A. Cocks, On the representation of random packings of spheres for sintering simulations, *Acta Metall. Mater.* 43 (1994) 3873–3884.
- [2] M. Bargiel, J. Moscinski, C-language program for the irregular dose packing of hard spheres, *Comput. Phys. Commun.* 64 (1991) 183–192.
- [3] N. Belheine, J.P. Plassiard, F.V. Donze, F. Darve, A. Seridi, Numerical simulation of drained triaxial test using 3D discrete element modeling, *Comput. Geotech.* 36 (1–2) (2009) 320–331.
- [4] M. Borkovec, W. de Paris, The fractal dimension of the Apollonian sphere packing, *Fractals* 2 (1994) 521–526.
- [5] F. Camborde, C. Mariotti, F.V. Donze, Numerical study of rock and concrete behaviour by discrete element modelling, *Comput. Geotech.* 27 (4) (2000) 247–257.
- [6] S. Pion, M. Teillaud, 3D Triangulations, CGAL User and Reference Manual, 3.5 edition, CGAL Editorial Board, 2009, http://www.cgal.org/Manual/3.5/doc_html/cgal_manual/packages.html#Pkg:Triangulation3.
- [7] P.A. Cundall, O.D.L. Strack, The distinct numerical model for granular assemblies, *Geotechnique* 29 (1) (1979) 47–65.
- [8] G. Cusatis, D. Pelessone, J.T. Baylot, Dynamic Pull-out Test Simulations Using the Lattice Discrete Particle Model (LDPM), *Proceedings of the 2008 ASCE Structures Congress*, 24–26, Vancouver, Canada, April, 2008.
- [9] F.V. Donze, V. Richefeu, S.A. Magnier, Advances in discrete element method applied to soil, rock and concrete mechanics, *State Art Geotech. Engrg. Electron. J. Geotech. Engrg.* 8 (2009) 1–44.
- [10] G. Frenning, V. Richefeu, S.A. Magnier, An efficient finite/discrete element procedure for simulating compression of 3D particle assemblies, *Comput. Meth. Appl. Mech. Engrg.* 197 (2008) 4266–4272.
- [11] W. Fujun, C. Jiangang, Y. Zhenhan, A contact searching algorithm for contact-impact problems, *Acta Mech. Sin.* 16 (4) (2000) 374–382.
- [12] P.L. George, On delaunay-based three dimensional automatic mesh generator, *Finite Elem. Anal. Des.* Vol. 25 (1997) 297–317. (<http://www-c.inria.fr/gamma/ghs3d/ghs.php>).
- [13] C. Geuzaine, J.-F. Remacle, Gmsh: A three-dimensional finite element mesh generator with built-in pre- and post-processing facilities, *Finite Elem. Anal. Des.* Vol. 1 (1) (2002) <http://www.geuz.org/gmsh/>.
- [14] S. Hentz, F.V. Donze, L. Daudeville, Discrete element modelling of concrete submitted to dynamic loading at high strain rates, *Comput. Struct.* 82 (29–30) (2004) 2509–2524.
- [15] J.-F. Jerier, D. Imbault, F.-V. Donze, P. Doremus, A geometric algorithm based on tetrahedral meshes to generate a dense polydisperse sphere packing, *Granular Matter* 11 (2009) 43–52.
- [16] W. Jodrey, E. Tory, Computer simulation of close random packing of equal spheres, *Phys. Rev. A* 32 (1985) 2347–2351.

- [17] R. Jullien, P. Meakin, Computer simulations of steepest descent ballistic deposition, *Colloids Surf. A Physicochem. Engrg. Aspects* 165 (2000) 405–422.
- [18] R. Kadushnikov, E. Nurkanov, Investigation of the density characteristics of three-dimensional stochastic packs of spherical particles using a computer model, *Powder Metall. Met. Ceram.* 40 (2001) 229–235.
- [19] J. Kozicki, F.V. Donze, Applying an open-source software for numerical simulations using finite element or discrete modelling methods, *Comput. Methods Appl. Mech. Engrg.* 197 (2008) 4429–4443.
- [20] J. Kozicki, F.V. Donze, YADE-OPEN DEM: an open-source software using a discrete element method to simulate granular material, *Engrg. Comput.* 26 (7) (2009) 786–805.
- [21] L. Liu, Y. Yuan, Dynamic simulation of powder compact by random packing of monosized and polydisperse particles, *J. Mater. Sci. Lett.* 19 (2000) 841–843.
- [22] B. Lubachevsky, F. Stillinger, Geometric properties of random disk packings, *Stat. Phys.* 60 (1990) 561–583.
- [23] S.A. Magnier, F.V. Donze, Numerical simulation of impacts using a discrete element method, *Mech. Cohes.-Friction. Mater.* 3 (3) (1998) 257–276.
- [24] C.L. Martin, Elasticity, fracture and yielding of cold compacted metal powders, *J. Mech. Phys. Solids* 52 (2004) 1691–1717.
- [25] C.L. Martin, D. Bouvard, S. Shima, Study of particle rearrangement during powder compaction by the discrete element method, *J. Mech. Phys. Solids* 51 (27) (April 2003) 667–693.
- [26] I. Marzec, J. Bobinski, J. Tejchman, Simulations of crack spacing in reinforced concrete beams using elastic-plasticity and damage with non-local softening, *Comput. Concr.* 4 (2007) 377–403.
- [27] MATLAB®, <http://www.mathworks.com>.
- [28] N. Monteiro Azevedo, J.V. Lemos, J. Rocha de Almeida, Influence of aggregate deformation and contact behaviour on discrete particle modelling of fracture of concrete, *Eng. Fract. Mech.* 75 (6) (2008) 1569–1586.
- [29] G. Mueller, Numerically packing spheres in cylinders, *Powder Technol.* 159 (2005) 105–110.
- [30] J.P. Plassiard, N. Belheine, F.V. Donze, A spherical discrete element model: calibration procedure and incremental response, *Granular Matter* 11 (5) (2009) 293–306.
- [31] V. Richefeu, M.S. El Youssofi, F. Radjai, Shear strength properties of wet granular materials, *Phys. Rev. E* 73 (2006) 051304.
- [32] V. Richefeu, M.S. El Youssofi, R. Peyroux, C. Bohatier, A model of capillary cohesion for numerical simulations of 3D polydisperse granular media, *Int. J. Numer. Anal. Methods Geomech.* 32 (11) (2008) 1365–1383.
- [33] V. Richefeu, M.S. El Youssofi, F. Radjai, Shear strength of unsaturated soils: Experiments, DEM simulations, and micromechanical analysis, proceedings in physics, *Theoretical and Numerical Unsaturated Soil Mechanics*, 113, Springer, 2007, pp. 83–91.
- [34] J. Rousseau, E. Frangin, P. Marin, L. Daudeville, Damage prediction in the vicinity of an impact on a concrete structure: a combined FEM/DEM approach, *Comput. Concr.* (2008) 343–358.
- [35] J. Schoberl, Netgen: an advancing front 2d/3d mesh generator based on abstract rules, *Comput. Visual Sci.* 1 (2000) 41–52. <http://www.hp fem.jku.at/netgen/>.
- [36] L. Scholtes, B. Chareyre, F. Nicot, F. Darve, Micromechanics of granular materials with capillary effect, *Int. J. Engrg. Sci.* 47 (1) (2009) 64–75.
- [37] W. Shiu, F.V. Donze, L. Daudeville, Penetration prediction of missiles with different nose shapes by the discrete element numerical approach, *Comput. Struct.* 86 (2008) 2079–2086.
- [38] L. Sibille, F. Nicot, F.V. Donze, F. Darve, Material instability in granular assemblies from fundamentally different models, *Int. J. Numer. Anal. Methods Geomech.* 31 (3) (2007) 457–481.
- [39] P. Stroeven, M. Stroeven, Dynamic computer simulation of concrete on different levels of the microstructure, *Comput. Simul. Concr.* 22 (2003) 1–10.
- [40] Y. Tan, D. Yang, Y. Sheng, Discrete element method (DEM) modeling of fracture and damage in the machining process of polycrystalline sic, *J. Eur. Ceram. Soc.* 29 (2009) 1029–1037.
- [41] A.R. Kansal, S. Torquato, F.H. Stillinger, Computer generation of dense polydisperse sphere packings, *J. Chem. Phys.* 117 (2002) 8212–8218.
- [42] C. Voivret, J.-Y. Delenne, M.S. El Youssofi, F. Radjai, Morphology of polydisperse granular media, *Traffic and Granular Flow 2007*, Springer, 2007, pp. 587–596.
- [43] C. Voivret, F. Radjai, J.-Y. Delenne, M.S. El Youssofi, Multiscale force networks in highly polydisperse granular media, *Phys. Rev. Lett.* 102 (2009) 178001.
- [44] R.Y. Yang, R.P. Zou, A.B.Yu. Computer, Simulation of the packing of one particles, *Phys. Rev. E* 62 (3) (2000) 3900–3908.
- [45] K.Z.Y. Yen, T.K. Chaki, A dynamic simulation of particle rearrangement in powder packings with realistic interactions, *J. Appl. Phys.* 71 (7) (1992) 3164–3173.